CHAPTER 3

EXPERIMENTAL SYNTHESIS, METHODS AND RESULTS

SYNTHESIS, CHARACTERIZATION, AND BASE CATALYSIS OF NOVEL ZEOLITE SUPPORTED SUPER—BASIC MATERIALS

3.1 Experimental synthesis and methods

Unless noted otherwise, all water is double distilled and deionized and all gases are passed over molecular sieves for water and oxygen removal prior to introduction to any reaction vessel.

3.1.1 Purification of solvents

O-xylene and toluene were dried and purified from anhydrous precursors. Toluene and *o*-xylene were refluxed over potassium metal for two hours under an inert blanket before distillation into an airless flask loaded with dehydrated 3A molecular sieves and stored in an inert atmosphere dry box.

3.1.2 Synthesis of zeolite LTL

Iron-free zeolite LTL was synthesized in the ratio 10 K_2O:1 Al_2O_3:25 SiO_2:400 H_2O according to Tsapatsis and co-workers.[1-3] A potassium aluminate solution was made from 22 mL KOH (Aldrich, 45 wt%) diluted to 150 mL with water and heated to 65^oC before addition of 3.61 g aluminum foil (Aldrich, 99.9995+%). A silicate solution was

obtained by diluting 44 mL KOH to 300 mL in water and slowly adding 9.99 g Cabosil M-5 to 30 mL of the KOH solution with stirring to form a white gel. Both solutions were allowed to stir overnight. A 15 mL aliquot of the potassium aluminate solution and 3.08 g H_2O were added the silica gel and stirred for 30 minutes. The synthesis gel was transferred to a Teflon lined autoclave under autogenous pressure in a 175^oC oven with rotation of 30 – 60 RPM for 8 hours. The mother liquor was removed following centrifugation and the solids were diluted with water. The was repeated four times prior to filtration by Buchner funnel. The resulting solids were dried at 110^oC overnight. Despite repeated attempts to synthesize pure phase LTL, X-ray diffraction shows that LTL was synthesized in mixed phase (data not shown).

3.1.3 Alkali-ion exchange of zeolite X

Ion exchange was performed on all zeolite samples prior to further processing to remove any manufacturing impurities and to be sure that only the desired cation was present. Some samples were calcined at 600^oC in air prior to ion exchange by ramping at 1 K/min to 250^oC, holding for 2 hours, and then ramping to 600^oC at 5 K/min for 12 hours. Procedures for ion exchange were adapted from Kim et al.[4] Enough NaX Strem Chemicals, Si/Al = 1.25) was added to a 0.1 N solution of NaOH (Aldrich, 97%), NaCl (Aldrich, 98+%), KOH (Aldrich, 85%), or CsOH (Aldrich, 95%), to create a slurry of 0.02 g zeolite/mL water. The slurry was stirred for 24 hours at room temperature, after which time the zeolite was separated by filtration and added to a fresh hydroxide solution. This procedure was repeated three times. The final slurry was agitated for 96 hours before

filtration. After drying for 24 hours at 100°C, the exchanged zeolite was analyzed by XRD, TGA, and elemental analysis. Aging of the sample was performed at 100°C for various amounts of time.

3.1.4 Occlusion of alkali—metal oxides

Alkali—metal oxides were occluded within pores of zeolite X following the work of Kim et al.[4] A 150 mL solution of 0.4 M or 1.5 M potassium acetate or cesium acetate, and 3 g sodium exchanged potassium or cesium exchanged zeolite X, respectively, was stirred for 24 hours at room temperature, after which time the zeolite was separated by filtration and added to a fresh solution of alkali acetate. This procedure was repeated three times. The final slurry was agitated for 96 hours before filtration. After drying for 24 hours at 100°C, the occluded alkali acetate was thermally decomposed under nitrogen. After an initial hold time of two hours at room temperature, temperature was raised at 1 K/min to 250°C and held for four hours before ramping to a final temperature of 455°C at 1 K/min and holding for 10 hours. Solids are denoted $(Y)M_1O_x/M_2X$ where Y denotes the molarity of the alkali acetate precursor solution, M_1 denotes the identity of the alkali—metal from the acetate solution, and M_2 denotes the cation of the exchanged zeolite. The solid $(1.5)CsO_x/CsX$ corresponds to cesium oxide impregnated into cesium exchanged zeolite X by 1.5M solution of cesium acetate. FTIR spectra of the samples as-made verify the presence of the acetate with bands at 1653 cm^{-1}, 1576 cm^{-1}, 1409 cm^{-1}, and 1343 cm^{-1}, consistent with data reported by Kim et al.[4] The onset temperature of decomposition for

CsO_x/CsX is consistent with previous studies.[5,6] Potassium acetate impregnated samples decomposed between 300 and 400°C by TGA analysis.

3.1.5 Synthesis of potassium azide

Synthesis of potassium azide was adapted from Beres et al.[7] To a slurry of 71.5 g NaN_3 (Aldrich, 99%) in 1000 mL water was added 148.16 g Bio-Rad AG1-X2 anion exchange resin in the acetate form. After agitation for 24 hours, the slurry was packed into a 3" diameter by 15" tall exchange column and rinsed with 3 L water to remove sodium and acetate ions. A 1 M, 100 mL solution of potassium hydroxide was then passed through the exchange column and flushed with 300 mL water. The first 100 mL to elute were set aside. The next 300 mL were rotary evaporated to crystals, which were rinsed with pentane and filtered. After drying 24 hours at 100°C the crystals were verified as potassium azide by FTIR (ν_{as} 2036 cm^{-1}, ν_b 649 cm^{-1}), X-ray diffraction (Fig. 3.1), and TGA (data not shown).

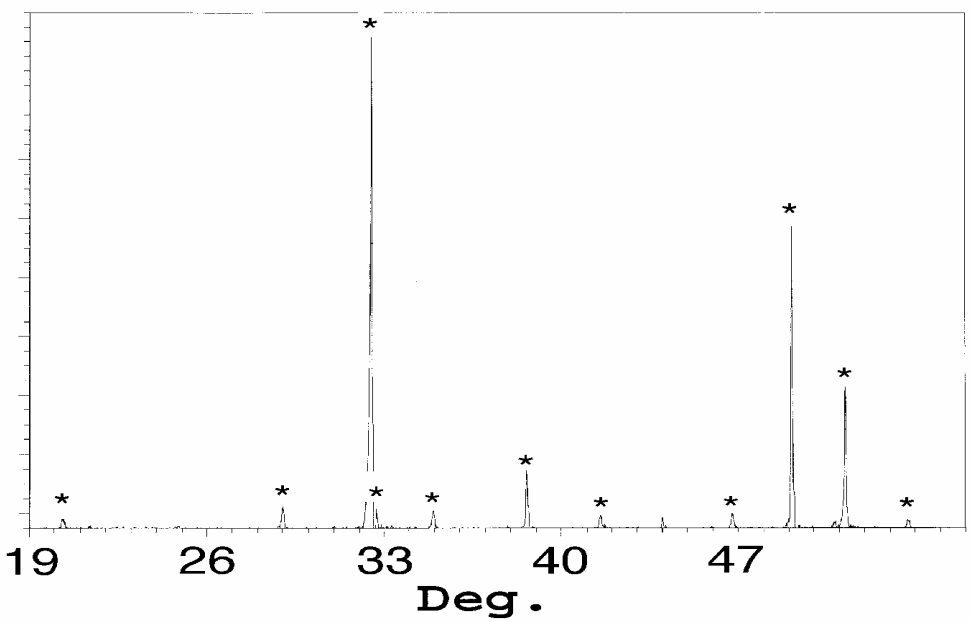

Figure 3.1: X-ray diffraction pattern of synthesized KN_3. Asterisks mark peaks matching the standard powder diffraction pattern for KN_3.

3.1.6 Occlusion of alkali—metal azides

The method of impregnation and decomposition of alkali—metal azides was adapted from Martens et al.[8] Variations in the method are depicted in Figure 3.2. Dry inert gas saturated with methanol was passed over a sample of dehydrated alkali exchanged zeolite X overnight. The minimum amount of methanol required to dissolve 1, 2.2 or 4.4 mmol azide/g zeolite, for nominal loadings of 2, 4, and 8 azides/supercage, respectively, was added to the dried azides. The methanolic azide solution was then added to ion-exchanged dehydrated or wet zeolite and allowed to stir under flowing argon overnight to evaporate the methanol. For the case of water based impregnation, the azide was dissolved in water prior to addition to the zeolite. The water was evaporated under vacuum. The

recovered solid was dried for 24 hours at 100^{o}C and characterized by XRD, IR, TGA, and high speed, solid-state 2D ^{23}Na MQMAS NMR. Solids are denoted (Y)M_1N_3/M_2X where Y is the synthesis loading of alkali—metal per zeolite supercage, M_1 is the identity of the alkali—metal in the alkali—metal azide, and M_2 is the exchange cation of zeolite X. The solid (4)NaN_3/KX denotes a loading of four additional sodium atoms per supercage of potassium exchanged zeolite X. Decomposition of the azide was performed in-situ just prior to reaction. After an initial hold time of two hours at room temperature, temperature was raised at 1 K/min to 250^{o}C and held for four hours to remove zeolitic water before ramping to a final temperature between 380 and 550^{o}C at 1 K/min and holding for between 5 and 10 hours.

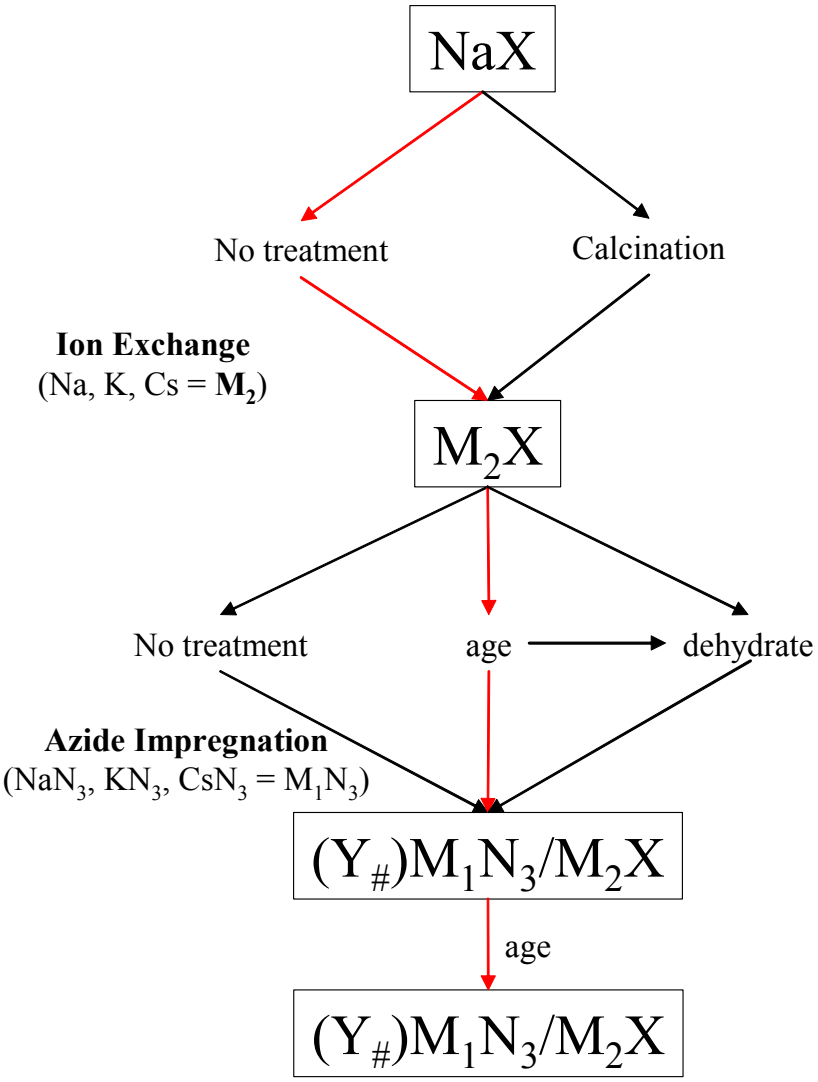

Figure 3.2: Synthesis routes for $(Y_{\#})M_1N_3/M_2X$. $Y_{\#}$ denotes the alkali azide loading level.

Alkali—metal alloys may be occluded within the zeolite pores using alkali—metal azides by impregnating alkali exchanged zeolites with azides of a different alkali—metal.[9,10] Electron exchange in the azide impregnated zeolites is opposite that of the gas phase.[9-12] The method of alloy formation is shown in Scheme 3.1. The azides NaN_3, KN_3, and NaN_3 were exchanged into each of NaX, KX, and CsX to produce metallic clusters and alloys following thermal decomposition of the azide precursors.

$$M_x^o + C^+ \rightarrow M_{x-1}^o + C^o + M^+$$

$$nC^o \rightarrow C_n^o$$

$$M_x^o + yC^+ \rightarrow (M_{x-y}^o C_y^o) + yM^+$$

Scheme 3.1: Mechanism for the formation of metallic alloys from alkali—metal azides impregnated in faujasite with a different exchange cation. M,C pairs denote (Na, K), (Na, Cs), or (Cs, K).

3.1.7 Alkali—metal azides supported on carbon molecular sieves

Carbon molecular sieves (CMS) with zeolite beta pore dimensions were obtained from Dow Chemical. The CMS were dehydrated by ramping at 1 K/min to 200^{o}C for 12 hr and then exposed to a stream of argon saturated with methanol vapor for two hours. Sodium azide, 0.165 g was dissolved into 10 mL methanol, added to the CMS, and stirred under flowing argon to remove the methanol. A black powder and white crystals were obtained. The white crystals were separated and identified as sodium azide by FTIR, TGA and XRD. Only trace amounts of sodium azide were incorporated into the CMS, as determined by FTIR and TGA analysis. This was mostly likely due to the lack of strong electrostatic interaction of the alkali—metal azide with the neutral CMS.

3.1.8 Semi—batch bulk-phase alkenylation and ethylation reactions

Alkenylation procedure was adapted from Doskocil et al.[13] Under the inert atmosphere of a dry box, a stir bar, 10 mL of *o*-xylene and either 10 μL NaK alloy (22 or

44% sodium, Aldrich), 0.010 g sodium (Aldrich, 99.95%), or 0.010 g potassium (Aldrich, 99.5%) metal were added to a 25 mL, 3-neck round bottom flask equipped with a Schlenk valve in one port. The remaining ports were closed with greased glass stoppers. After attachment to a vacuum line, the vacuum tube was evacuated and backfilled with Argon three times before opening to the reactor vessel. In the meantime, a condenser was also evacuated and backfilled with Argon three times. The condenser was then attached to the reactor vessel under flowing Argon and the remaining stopper was replaced with a septum. The completed apparatus is shown in Figure 3.3. The vessel was then heated to the reaction temperature of 143^{o}C while stirring and a flow of 2 mL/min butadiene diluted nine times with UHP (ultra high purity) Nitrogen (to reduce oligomerization of butadiene) was introduced to the vessel by 20 gauge syringe needle. Aliquots of 0.1 mL were taken after the first hour and every hour and a half thereafter by a syringe equipped with a 20 gauge needle. Both syringe and needle were taken from an oven at 150^{o}C and purged using argon in the head space of a dummy flask filled with argon just prior to sampling. Aliquots were diluted fifteen times in a solution of dichloromethane and methanol (15:1) before 1μL injection to a HP5890 Series II gas chromatograph equipped with a capillary HP-5 column and flame ionization detector or mass spectrometer. Diphenylmethane was used as an internal standard for GC calibrations. The following temperature program was used: initial temperature 40^{o}C, no hold time, 8^{o}C/min ramp rate to 280^{o}C final temperature for 5 minutes.

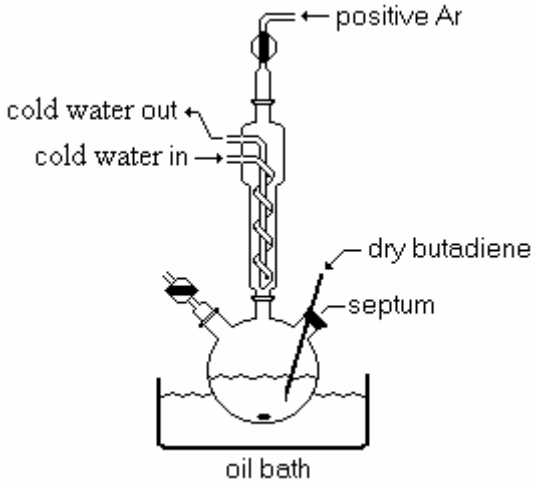

Figure 3.3: Reaction apparatus for bulk phase semi—batch reactions.

3.1.9 Semi—batch supported alkenylation and ethylation reactions

Initially, reactions with azide containing materials were performed by first thermally decomposing the azide in a U-tube separate from the reaction vessel and then transferring the sample to the reaction vessel under flowing argon following decomposition. Later decompositions were carried out in-situ under argon using the apparatus shown in Figure 3.4. Following activation, 10 mL dried *o*-xylene was loaded into a 25 mL round bottom flask in an inert atmosphere dry box and stirred over potassium for 30 minutes. The *o*-xylene was then introduced to the reaction vessel by dried and purged canula. The reaction vessel was heated to 143^{o}C while stirring and a flow of 2 mL/min butadiene diluted nine times with nitrogen was bubbled through the reaction mixture by needle. Aliquots for analysis were taken every 1.5 hours as described for bulk catalyst alkenylation and analyzed using a HP5971 mass spectrometer preceded by a HP-5 capillary GC column using the temperature program developed for bulk phase reaction.

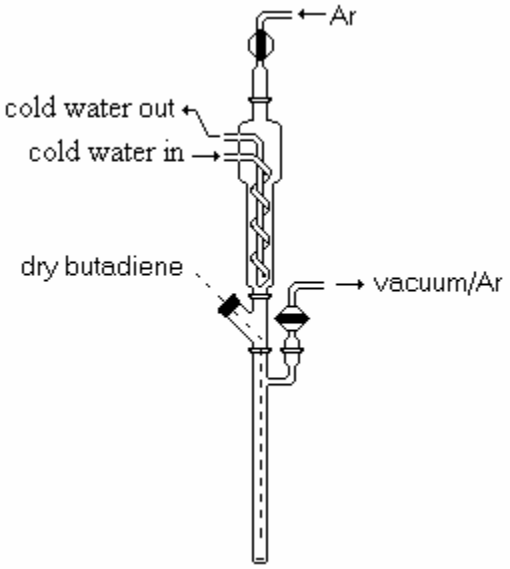

Figure 3.4: Zeolite supported base catalysis apparatus.

3.1.10 Gas—phase alkenylation and ethylation reactions

A gas—phase vertical flow reactor system was constructed for the isomerization of 1-butene, ethylation of *o*-xylene and alkenylation of *o*-xylene with 1,3-butadiene . A schematic is shown in Figure 3.5. Thermocouple placement along all transfer lines allowed accurate control of temperature. The butadiene cylinder and all transfer lines up until the *o*-xylene addition were heated to 50^{o}C to prevent condensation of butadiene. All lines containing *o*-xylene were heated to at least 150^{o}C. Gas phase ethylation procedures from Martens et al. were adopted for both *o*-xylene ethylation and alkenylation with butadiene.[14] Reactive flows consisted of dried and distilled *o*-xylene (1.2 hr^{-1} WHSV), 1,3-butadiene, and argon (Air Liquide, 99.999%) in a ratio of 5:1:2 1,3-butadiene:*o*-xylene:argon. Catalysts (0.5 g, ~1 mL) were pressed and size selected to 35/60 mesh and diluted to 3 mL with 16 mesh silicon carbide (Abrasives Unlimited). The catalyst mixture was supported

between steel wool plugs in the center of a ½" diameter steel reactor tube and thermally activated under 16 mL/min argon flow. After three hours at 30^{o}C, temperature was ramped to 250^{o}C at 1.5 K/min for six hours to remove zeolitic water, ramped to 380^{o}C < T < 550^{o}C at 1 K/min for 5 - 10 hours and then ramped to the reaction temperature at 1 K/min. The reaction was sampled by online GC equipped with a 30 m HP-5 capillary column and a flame ionization detector following the program previously developed. No products were observed over the SiC diluent under reactive conditions.

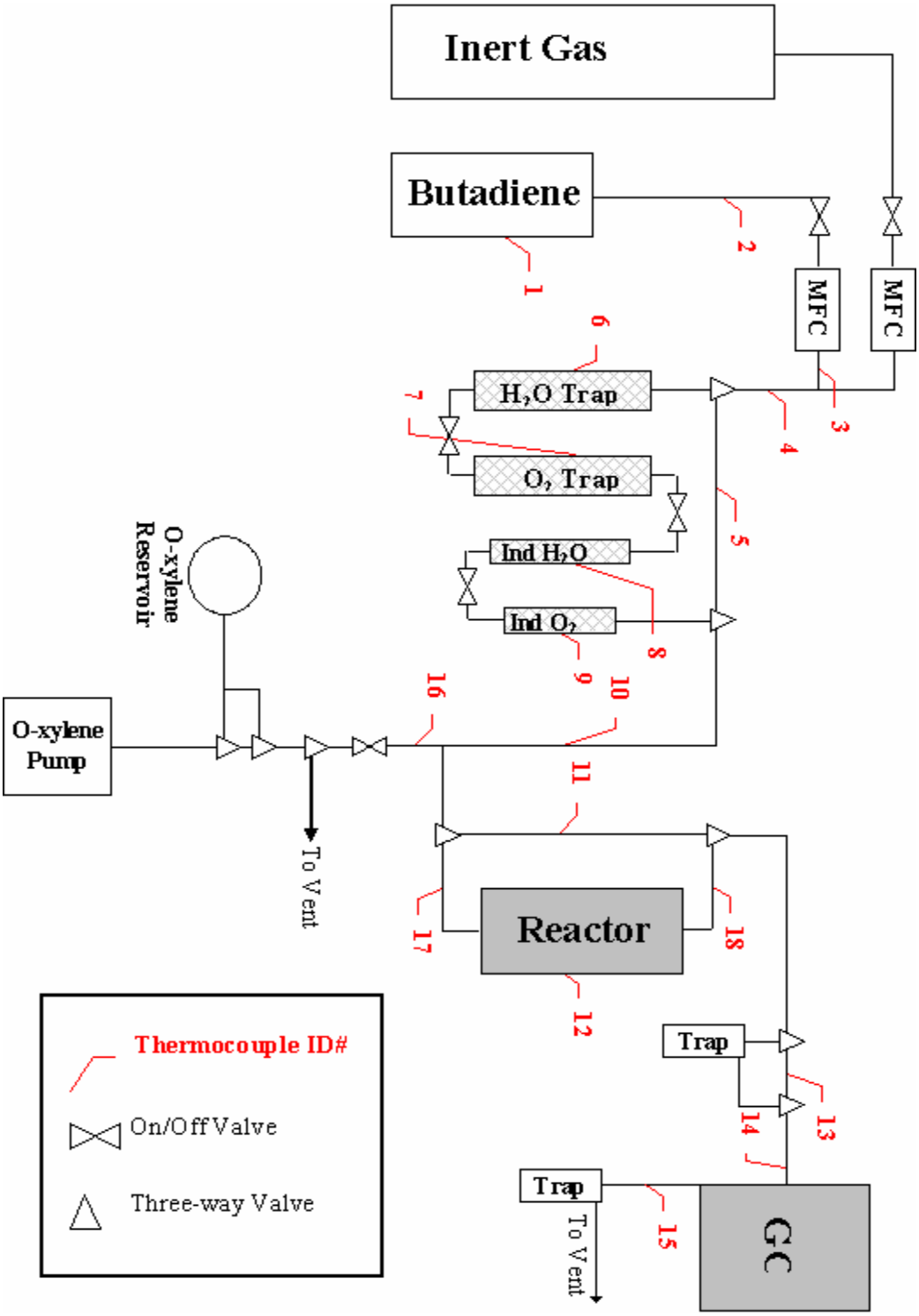

Figure 3.5: Gas phase reaction system with thermocouple locations on heated elements of the reactor apparatus. MFC = mass flow controller, GC = gas chromatograph, Ind = indicating.

3.1.11 Gas—phase isomerization of 1-butene

The gas phase isomerization of 1-butene was performed over alkali-loaded zeolites using the apparatus described above. Reactive flows for both acetate and azide containing precursors consisted of a 9:1 ratio of argon:1-butene and total flow rate of 10 mL/min. Activation of alkali containing materials was adopted from the studies of Bordawekar et al.[5] The reactor was loaded with 0.5 g 35/60 mesh size selected catalyst diluted to 3 mL with silicon carbide as described above. Activation was performed under 10 mL/min argon. After 8.5 hours at 30^{o}C, the temperature was ramped at 2 K/min to 250^{o}C for two hours, ramped at 1 K/min to 500^{o}C for 5 hours and then ramped to the reaction temperature of 100^{o}C at 1.5 K/min. Azide containing precursors were size selected to 35/60 mesh, diluted to 3 mL with silicon carbide and loaded into the reactor as previously described. After seven hours at 30^{o}C, the temperature was ramped at 2 K/min to 250^{o}C for six hours, ramped at 1 K/min to 380^{o}C for 5 hours, and then ramped at 2 K/min to the reaction temperature of 150^{o}C. Products were detected by a GC equipped with a 100 m petrocol capillary column and flame ionization detector by ramping from 50^{o}C to 250^{o} at 10 K/min and holding at 250^{o}C for 10 minutes.

3.1.12 Characterization

A Netzsch STA 449C Jupiter system was used to record simultaneous thermogravimetric analyses (TGA) and differential scanning calorimetry (DSC). Samples

were loaded into platinum/rhodium crucibles and heated to 900°C at 1 K/min under 50mL/min inert gas. Infrared spectra were recorded on a Nicolet Nexus 470 FTIR spectrometer using KBr wafers of approximately 1 wt% solid in KBr. Powder X-ray diffraction (XRD) was performed on a Scintag XDS 2000 diffractometer using a liquid nitrogen cooled germanium crystal detector and CuKα radiation.

Solid-state magic angle spinning (MAS) spectra were recorded on a Bruker Avance 500 spectrometer at a spinning rate of 12 or 14 kHz. ^{23}Na NMR spectra were recorded at 132.3 MHz. The ^{23}Na 2D MQMAS experiments were performed using the standard *z*-filtered sequence[15] with proton decoupling. Pulse widths for the excitation of the triple quantum coherence, refocusing, and selective readout were 4, 1.4 and 8 μs, respectively. A recycle delay of 0.3 s was used. Samples were dehydrated or thermally activated prior to use and loaded into the NMR rotor in a nitrogen atmosphere glove box.

3.2 Results

3.2.1 Characterization

Alkali azide containing materials were characterized by FTIR, TGA, solid-state MAS NMR, and X-ray diffraction. X-ray diffraction measurements show that the framework of zeolite X is intact following incorporation of the azide species and following thermal decomposition of the azides at 550°C. Representative FTIR spectra acquired at room temperature for sodium exchanged zeolite X, sodium azide, (2)NaN_3/NaX, and

(4)NaN_3/NaX are shown in Figure 3.6. Asymmetric stretches at 2126 cm^{-1} (broad) with a sharp shoulder at 2036 cm^{-1} are characteristic of sodium azide (line d). Sodium exchanged sodium X zeolite shows no peaks in the range indicative to azide stretching (line a). When sodium azide is occluded within the pores of zeolite X, the broad asymmetric stretching peak of the azide is resolved into two separate asymmetric stretching bands at 2130 cm^{-1} and 2056 cm^{-1}, indicating that the stretching vibrations have been restricted by occlusion of the azide within the zeolite pores. Splitting of the asymmetric stretching bands at room temperature has been observed elsewhere and is attributed to the partitioning of the azide ion into distinct crystallographic locations within the zeolite.[16-18] The band at 2130 cm^{-1} is due to azide occluded within the sodalite cages of faujasite, while the band at 2056 cm^{-1} is due to azide occluded within the supercages of faujasite. The band at 2037 cm^{-1} is attributed to extra lattice azide, and is eclipsed by the band at 2056 cm^{-1} in (4)NaN_3/NaX. These results verify occlusion of the alkali azide species within the pores of the zeolite.

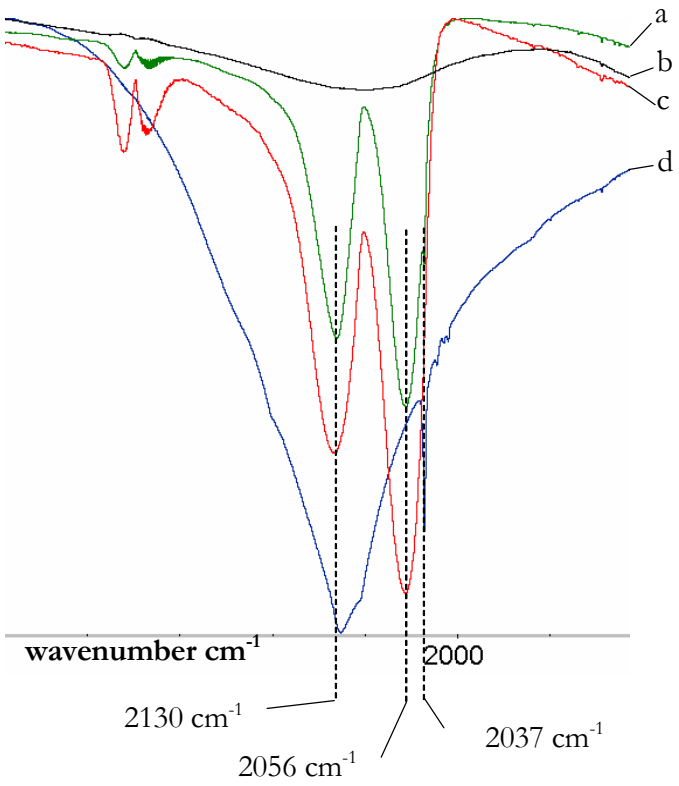

Figure 3.6: FTIR spectra of a) (2)NaN_3/NaX, b) NaX, c) (4)NaN_3/NaX, d) NaN_3 in KBr.

Representative TGA/IR analyses for (Y)NaN_3/NaX (Y = 2, 4) are shown in Figure 3.7, along with TG data for sodium exchanged NaX. The amount of water desorbed from the zeolite decreases with increased azide loading, indicating that the azide is replacing water in the pores of the zeolite. The (Y)NaN_3/NaX samples show a secondary weight loss beginning at 380°C and continuing past 700°C. FTIR spectra confirm that this weight loss is due to removal of the azide from the zeolite. The slow decomposition of the azide within the zeolite pores is in stark contrast to its extremely rapid weight loss in the bulk phase, but consistent with other studies.[7,17]

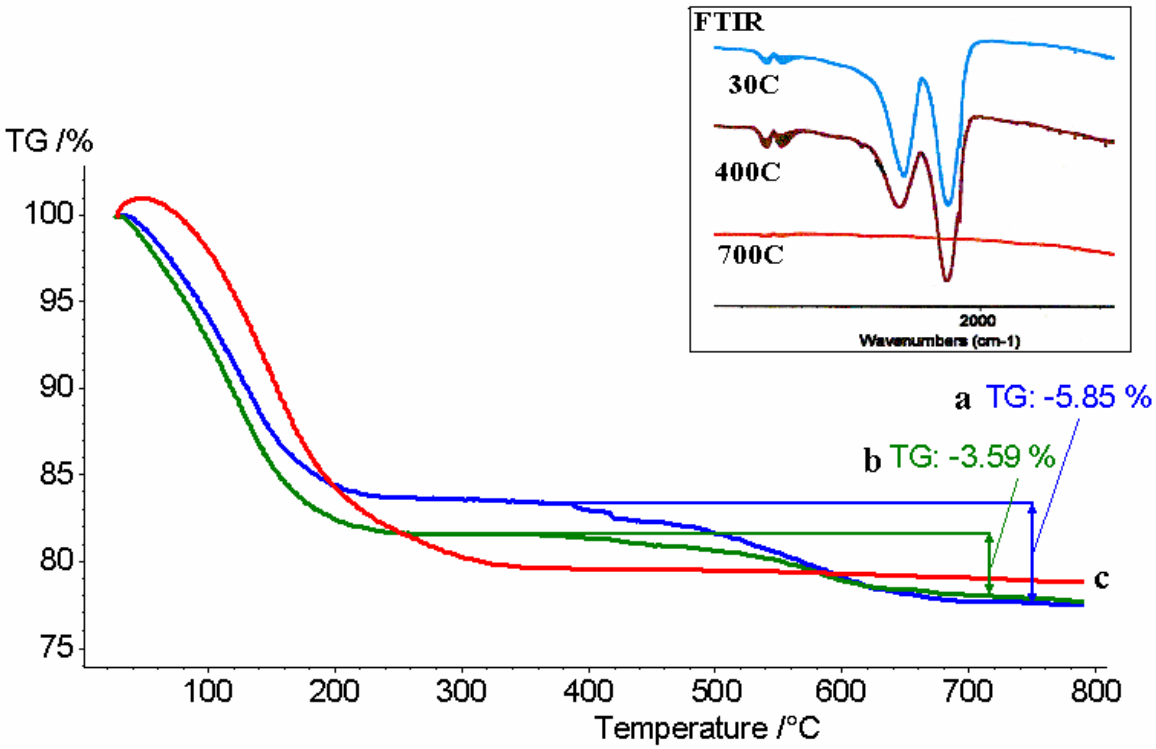

Figure 3.7: TGA and IR (inlay) analyses of a) (4)NaN_3/NaX, and b) (2)NaN_3/NaX c) NaX.

Despite the absence of detectable nitrogen species by FTIR after decomposition at 700°C, the TGA data for azide occluded zeolites indicate an incomplete mass balance based on decomposition of the azide to nitrogen gas and alkali—metal. Data for several azide containing zeolites are shown in Table 3.1. The mass deficit following thermal decomposition of the azides has been noted elsewhere and assigned to missing nitrogen by ^{15}N NMR,[14] EPR,[18] and high temperature IR measurements.[17,18] The residual nitrogen can be observed by IR and is thought to form N-O species with the zeolite framework, "gluing" the metallic sodium clusters to the zeolite framework and giving rise to unusual thermal stability of the metallic clusters (Fig 3.8).[18] Indeed, after decomposition at 550°C for 10 hours under helium, (4)NaN_3/NaX shows three bands of non-negligible intensity at

2030cm^{-1}, 2171cm^{-1}, and 2242cm^{-1} (Fig. 3.9). These have been attributed to the linear and bridged forms of the N-O species pictured in Figure 3.8.[18] It has also been proposed that the bands are due to salt occlusion of the azide after ion exchange of azide sodium for a proton on residual Brønstead OH groups within the zeolite.[7,17-20] However, it has been shown that salt occlusion of the azide is an intermediate step to the formation of N-O anchor species.[16]

Sample	% Mass Loss	Expected % Loss	% Deficit
(2)NaN3/NaX	3.59	3.77	4.8
(4)NaN3/Nax	5.85	6.97	16.0
(2)KN3/NaX	3.30	4.00	17.5

Table 3.1: Results from TGA of occluded alkali—metal azides under nitrogen atmosphere ramping at 1 K/min.

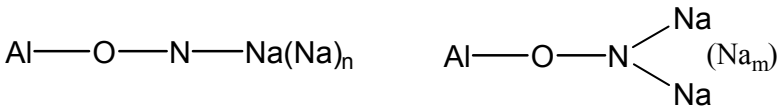

Figure 3.8: Possible anchor structures of metallic sodium clusters in zeolite pores following thermal decomposition of the azide.

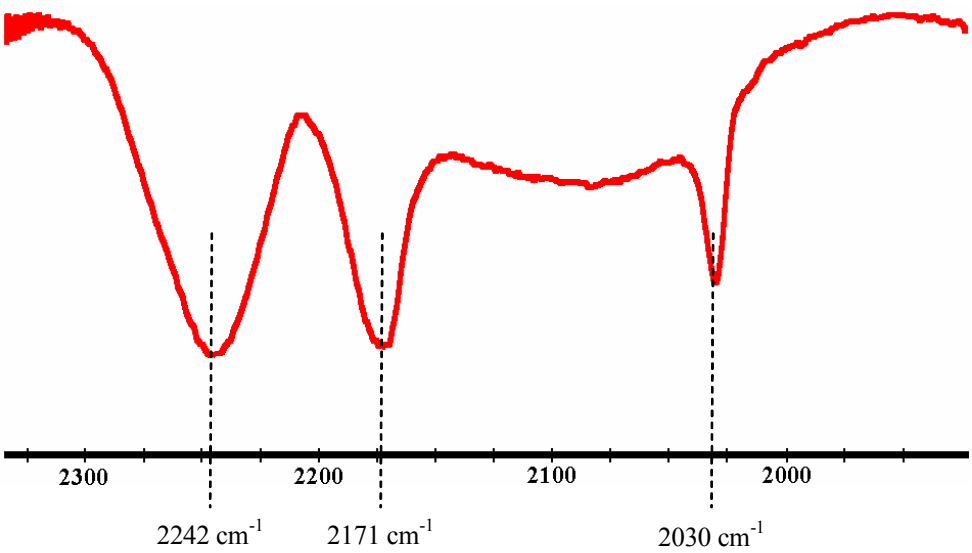

Figure 3.9: FTIR spectrum of (4)NaN_3/NaX following azide decomposition at 550°C for 10 hours under flowing helium.

The results from IR and TGA analyses are corroborated by ^{23}Na 1D and 2D MQMAS NMR for samples loaded with sodium azide. In zeolite NaX there are five crystallographic distinct cation sites (Fig. 3.10) which can be visualized by both 1D MAS and 2D MQMAS ^{23}Na NMR.[21-23] Coupling high speed MAS NMR with simulation allows determination of location and site occupancy for the exchanged sodium cations. Information about the electronic environment around the sodium cations can be determined from the use of 2D MQMAS NMR. Spin-spin interaction information is available on the isotropic axis of collected 2D MQMAS NMR spectra. Chemical shift is measured on the anisotropic axis.

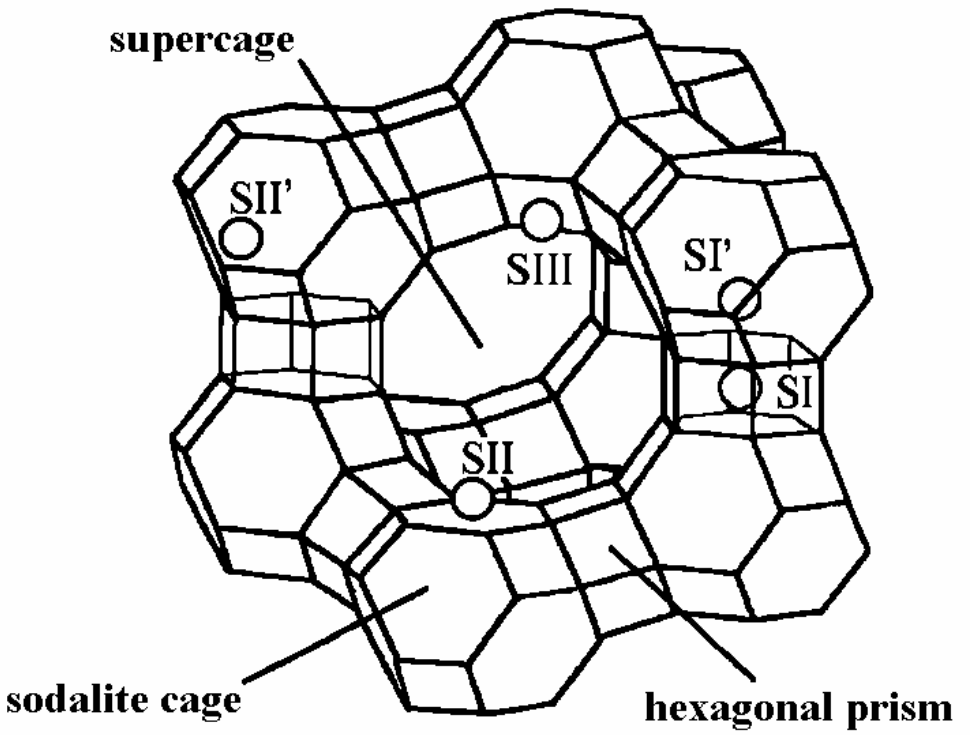

Figure 3.10: Projection of the cage structure of FAU showing potential cation locations, adapted from ref [[22]]. Site III' is composed of two slightly non-symmetrical sites; sites III'(1,2) and III'(3) are slightly off center of site III.

Figure 3.11 presents the solid state ^{23}Na 1D MAS NMR spectrum acquired for dehydrated sodium exchanged NaX. The five features of the signal in the 1D spectrum suggest that five cation sites are occupied, consistent with reports found in the literature.[21-24] These reports facilitate assignment of the peaks to specific crystallographic locations. Features characteristic of sites I and I' are found at -1.4 and -74.0 ppm, respectively. Site II is identified by the shoulder at -54.4 ppm. Sites III'(1,2) and III'(3) are located at -26.8 and -19.5 ppm, respectively. Simulation of the spectrum allows site occupancy to be determined. Results of simulation using the program QCC are found in Figure 3.12 and Table 3.2. The powder patterns characteristic of sites I' and II are the result of large

quadrupole coupling constants (Q_{cc}) and small asymmetry parameters (η). Simulation of the spectrum (Fig 3.12, Table 3.2) could not resolve the two contributions to site III, namely III'(1,2), and III'(3), despite repeated simulation attempts. This result is not unprecedented, however.[25] The occupancy of crystallographic sites, although a weak function of Si/Al ratio and hydration level, falls between values reported in the literature. Sites I and I' account for 6.6 and 27.5% occupancy, respectively. Site II accounts for 32.2% of sodium ions. The combined site III, III'(1,2) and III'(3), accounts for 34.2% of the occupancy, which is consistent with the sum of occupancies for sites III'(1,2) and III'(3) reported in the literature[22-24]. The values of Q_{cc} and η obtained for sites I, I', and II' fall within the range of values reported in the literature.[22-24] The same parameters obtained for the combined site III fall between the reported values for peaks III'(1,2) and III'(3).[22-24] Isotropic chemical shift is affected by the NMR program, Si/Al, and level of hydration. Thus, no meaningful comparison of the isotropic shift can be made. These combined data, however, indicate that assignment of peaks to crystallographic occupancy sites for zeolite NaX is possible by 1D NMR.

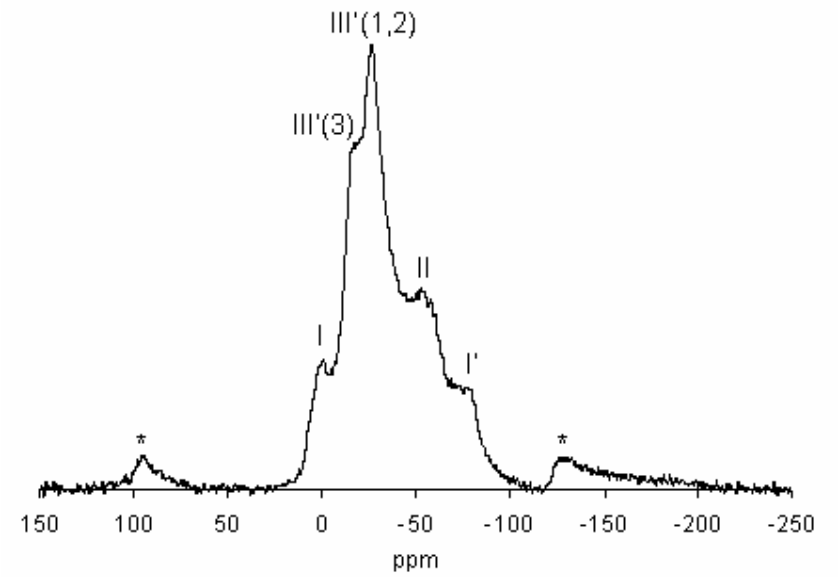

Figure 3.11: Solid state ^{23}Na MAS NMR of dehydrated NaX zeolite. Asterisks mark spinning sidebands.

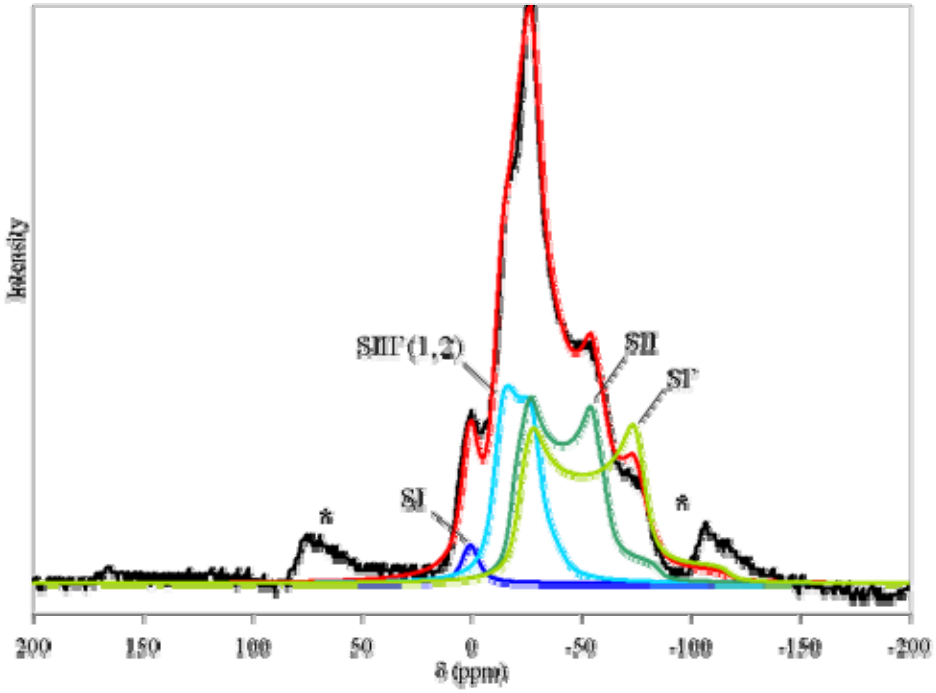

Figure 3.12: Simulated ^{23}Na MAS NMR spectrum confirming site assignments. Asterisks mark spinning sidebands on the observed spectrum. The two components of site III, III'(1,2) and III'(3), could not be resolved by simulation.

Site	Occ.	δiso (ppm)	$Qcc^a/Q_{cc}{}^b$ (MHz)	η^a/η^b	LB (Hz)
I	6.6%	3.5	1.5 / (1.4 ± 0.2)	0.1 / (0 - 0.1)	525
III	34.2%	-7.9	3.1 / (-)	0.2 / (-)	542
II	32.2%	-11.7	4.5 / (4.8 ± 0.2)	0.2 / (0 – 0.2)	392
I'	27.5%	-9.0	5.5 / (5.6 ± 0.4)	0.1 (0 - 0.1)	496

[a] results from simulation
[b] reported in references [22-24]

Table 3.2: Simulation results for dehydrated NaX zeolite.

Information about the local electronic environment around each cation site can be obtained from 2D MQMAS NMR. The ^{23}Na MQMAS NMR spectra for dehydrated NaX are shown in Figure 3.13. Projection of the collected 2D MQMAS spectra onto the isotropic axis indicate that there are at least four cation sites present in the sample, consistent with the 1D and simulation results. The sites are easily discernible, indicating that they are relatively well isolated from each other electronically. Powder patterns are clearly evident at ~20 and ~40 ppm along the isotropic axis. The symmetric peak visible at ~40 ppm along the isotropic axis is a spinning sideband. Peaks at -12 ppm and 8 ppm along the isotropic axis are mostly symmetrical. The fifth site identified by 1D MAS NMR is not well resolved by the 2D MQMAS technique.

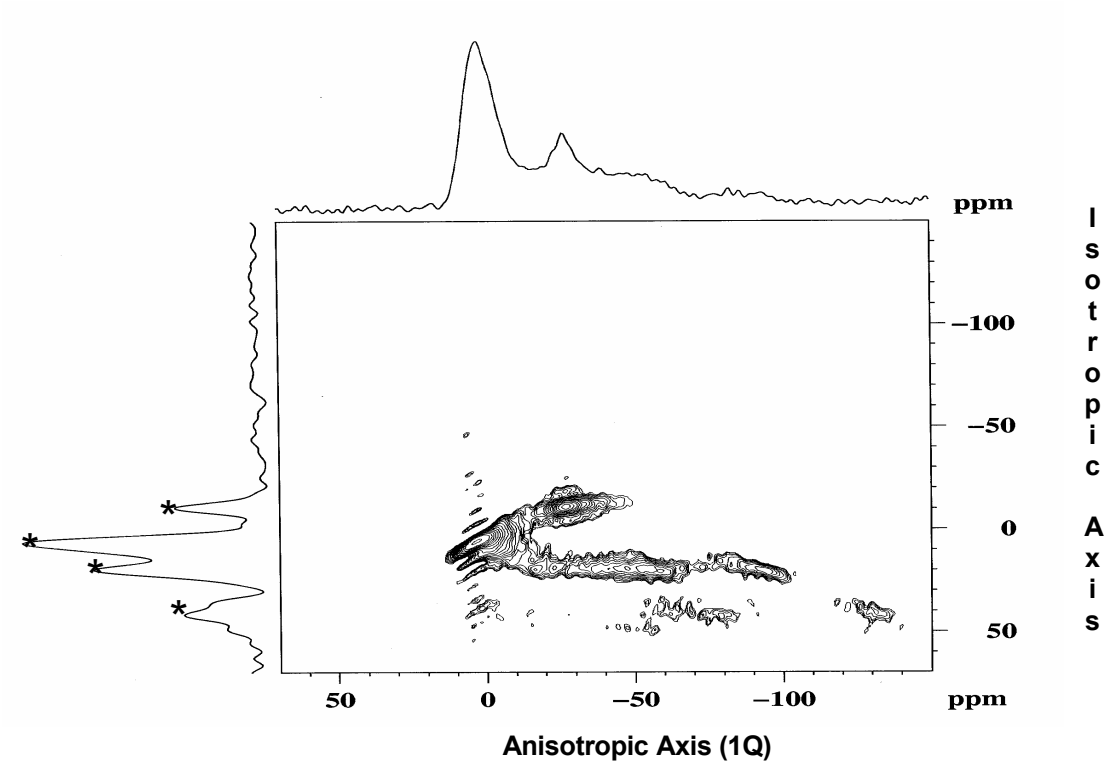

Figure 3.13: Solid state 2D MQMAS ^{23}Na NMR spectra acquired from dehydrated NaX zeolite. Asterisks on the projected isotropic axis mark cation sites. The symmetry of the marked sites is determined by examination of the 2D plot along the anistropic axis.

The scaled 1D spectra of NaX, (2)NaN_3/NaX, (4)NaN_3/NaX, and thermally decomposed (4)NaN_3/NaX, are shown in Figure 3.14. As sodium azide loading is increased, the intensities of sites III'(1,2), II, and I' decrease. The cause of migration to a selected few sites could be due to the steric constraints imposed on the cations by the increasing presence of azide within the zeolite pores. Indeed, NMR studies have shown that cations in FAU are mobile and easily affected by absorbed species.[23,24,26-28] The fact that several sites exist and participate in migration indicates that the azide must be occluded

within the pores of the zeolite after impregnation. Simulations of the spectra were not able to replicate the acquired data for alkali azide impregnated materials.

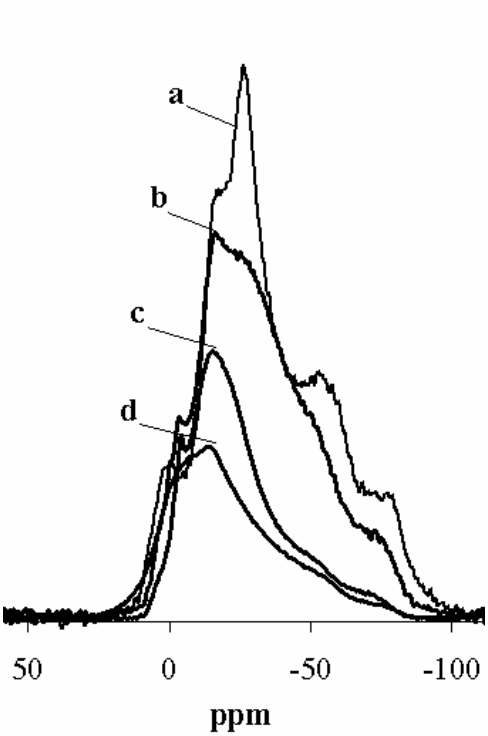

Figure 3.14: Scaled ^{23}Na 1D MAS NMR spectra for a) dehydrated NaX, b) (2)NaN_3/NaX, c) (4)NaN_3/NaX, and thermally activated (4)NaN_3/NaX.

Although NMR was not performed quantitatively, the amount of material loaded into the NMR rotor for each experiment varied by no more than 5 - 10%. Un-scaled peak areas for each of the curves in Figure 3.14 were not significantly affected by azide loading or decomposition. Thus, the presence of azide species within the pores is primarily responsible for cation redistribution, although some NMR silent paramagnetic ionic clusters may also be formed.[9,11,26,29,30] The difference in signal intensity between as-made and thermally decomposed (4)NaN_3/NaX suggests that very few cations are removed to NMR silent ionic clusters or metallic clusters, despite the expectation of metallic

clusters.[9,29,31-33] Although it is possible to determine the presence of neutral metallic sodium clusters[10,17,34] or alloys[32,35] within the zeolite by monitoring the NMR Knight shift characteristic of metals and alloys in the solid state NMR spectra, no peaks attributable to metallic sodium clusters or alloys were observed by MAS NMR in thermally decomposed alkali azide impregnated materials.

The number of unique cation species observed by analysis of the isotropic axis in ^{23}Na 2D MQMAS NMR spectra presented in Figures 3.15 - 3.17 decreases from 4 - 5 species for NaX to 1 - 3 species for as made and thermally decomposed (4)NaN_3/NaX, consistent with migration of the cation species suggested by ^{23}Na 1D MAS NMR. Peaks present in ^{23}Na MAS NMR and the number of potential cation sites visualized by ^{23}Na 2D MQMAS NMR are presented in Table 3.3. The 2D MQMAS NMR spectra show that the electronic isolation of the cation sites is greatly decreased by the introduction of sodium azide to the zeolite. In order for the azides to affect cation site distribution within the zeolite pores, the azide species must be present within the pores of the zeolite. Thus, these data show that the sodium azide is easily occluded within the pores of zeolite X.

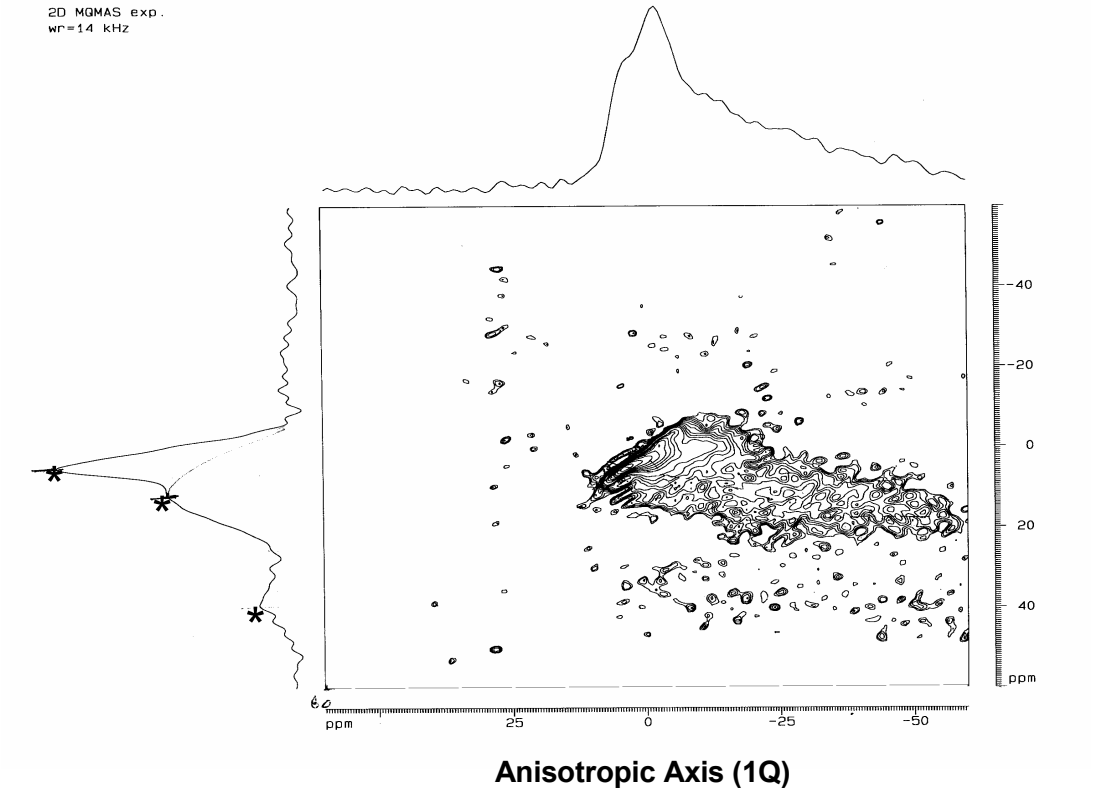

Figure 3.15: ^{23}Na 2D MQMAS NMR of as made (2)NaN_3/NaX showing a decrease in the unique number of cation sites when compared to dehydrated NaX. Asterisks on the projected isotropic axis mark potential unique cation sites.

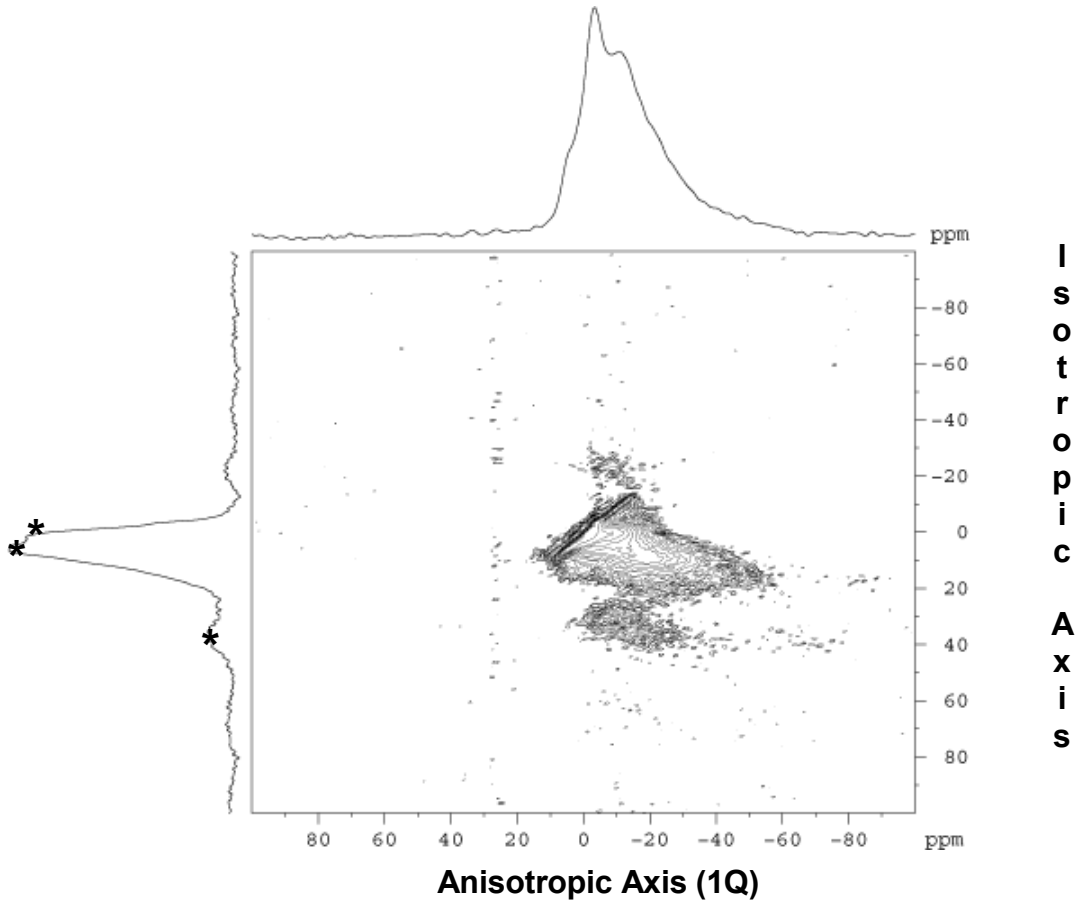

Figure 3.16: ^{23}Na 2D MQMAS NMR of as made (4)NaN_3/NaX showing a decrease in the unique number of cation sites when compared to dehydrated NaX. Asterisks on the projected isotropic axis mark potential unique cation sites.

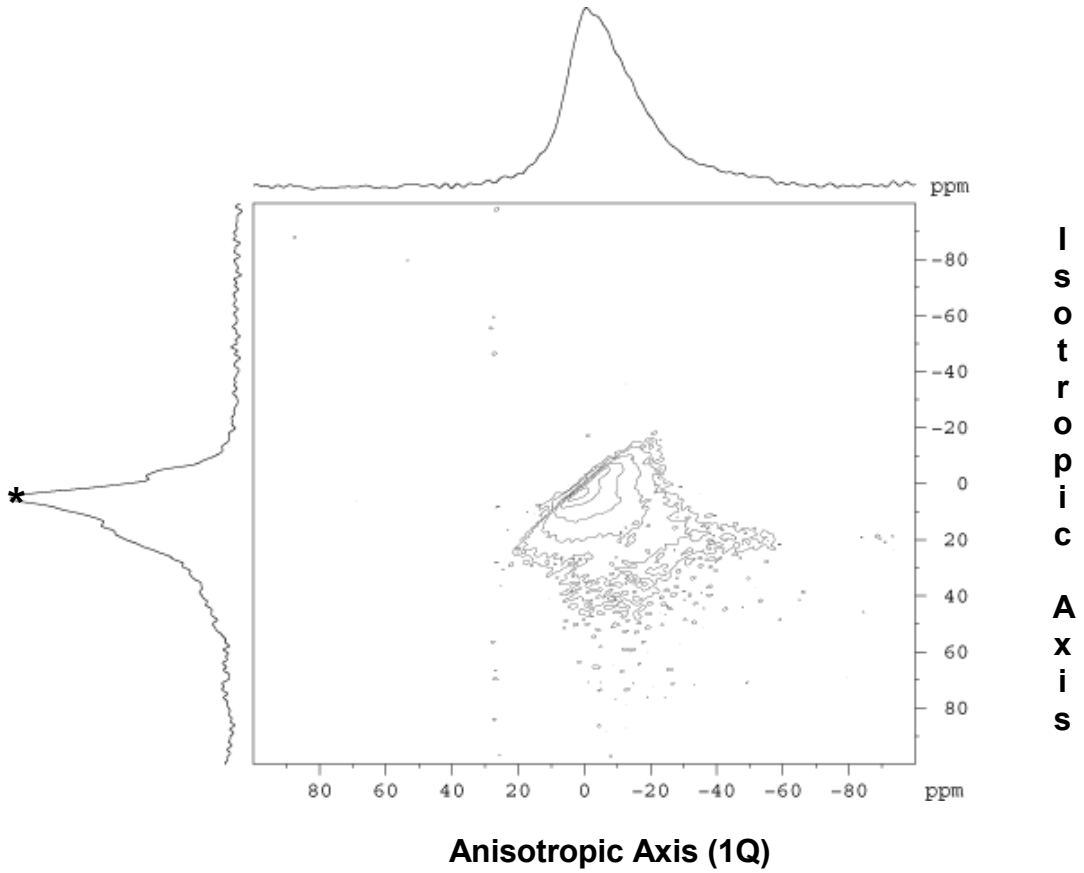

Figure 3.17: ^{23}Na 2D MQMAS NMR of thermally activated (4)NaN_3/NaX showing a decrease in the unique number of cation sites when compared to dehydrated NaX. Asterisks on the projected isotropic axis mark potential unique cation sites.

Catalyst	Potential Sites	Peaks (ppm)
NaX	4-5	-1.4, -19.5, -26.8, -54.4, -74.0
(2)NaN_3/NaX	3-4	-3.5, -16.0, -24.8, -50, -73
(4)NaN_3/NaX	1-3	-4.4, -16.7, -50, -70
(4)NaN_3/NaX*	1-3	-14.7, -50, -76

Table 3.3: Peak positions of ^{23}Na MAS NMR and possible number of unique cation sites determined by ^{23}Na 2D MQMAS NMR in dehydrated NaX, (2)NaN_3/NaX, (4)NaN_3/NaX, and thermally activated (4)NaN_3/NaX*.

3.2.2 Semi—batch bulk—phase alkenylation

The results from bulk phase semi—batch alkenylation of *o*-xylene with 1,3-butadiene over bulk sodium, potassium, and sodium/potassium alloys are plotted as selectivity (5-OTP) versus conversion in Figure 3.18. Products other than 5-OTP were formed from the subsequent addition of butadiene to *o*-xylene or the formation of the product "Z" (Scheme 3.2). The spread of data at low conversion is due to contamination of the catalyst during sampling and reactor transfer during early runs. These problems were eliminated at later times. The Na/K alloys and potassium were highly active and gave rise to almost identical selectivity curves. Sodium metal was inactive for alkenylation of *o*-xylene in the bulk phase, consistent with previous studies.[13] A red solution indicative of an organo—alkali species was present during alkenylation over any of the active catalysts. Despite following the same selectivity curve as NaK (44/56) and K metal, the NaK (22/78) eutectic exhibits the highest activity of the catalysts, with a turnover number (TON) of 125 vs. 105 and 107, respectively. However, the differences in TON could be due variations in exposed catalyst surface due to variable dispersion of the catalysts as opposed to synergy between sodium and potassium at the eutectic (22/78) composition. Selectivity to 5-OTP at 10% conversion is between 80 and 90% for all of the active catalysts, in agreement with previously published results for potassium[13] and the BP-Amoco commercial process.[36] No direct comparison could be found for NaK (44/56). The lack of activity over sodium metal and the absence of any variation in the selectivity versus conversion curve with composition of eutectic suggest that potassium is the active site for alkenylation of *o*-xylene in the bulk phase.

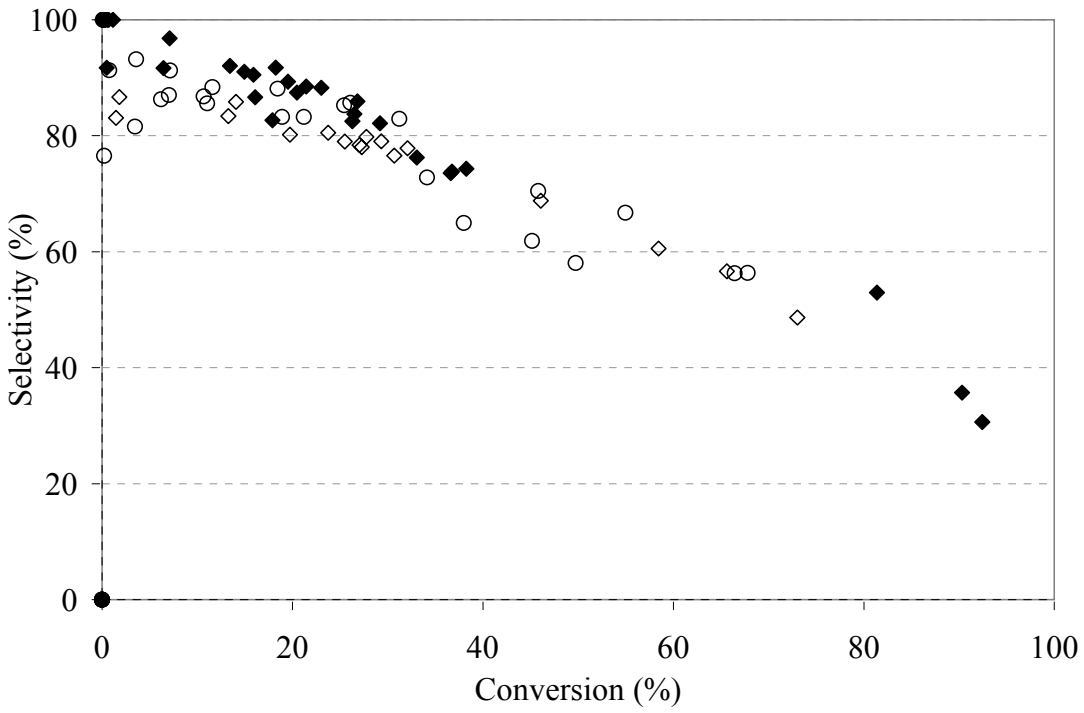

Figure 3.18: Selectivity versus conversion data for the semi—batch alkenylation of *o*-xylene with 1,3-butadiene over NaK (22/788, ♦), NaK (44/56, ◊) and K (○).

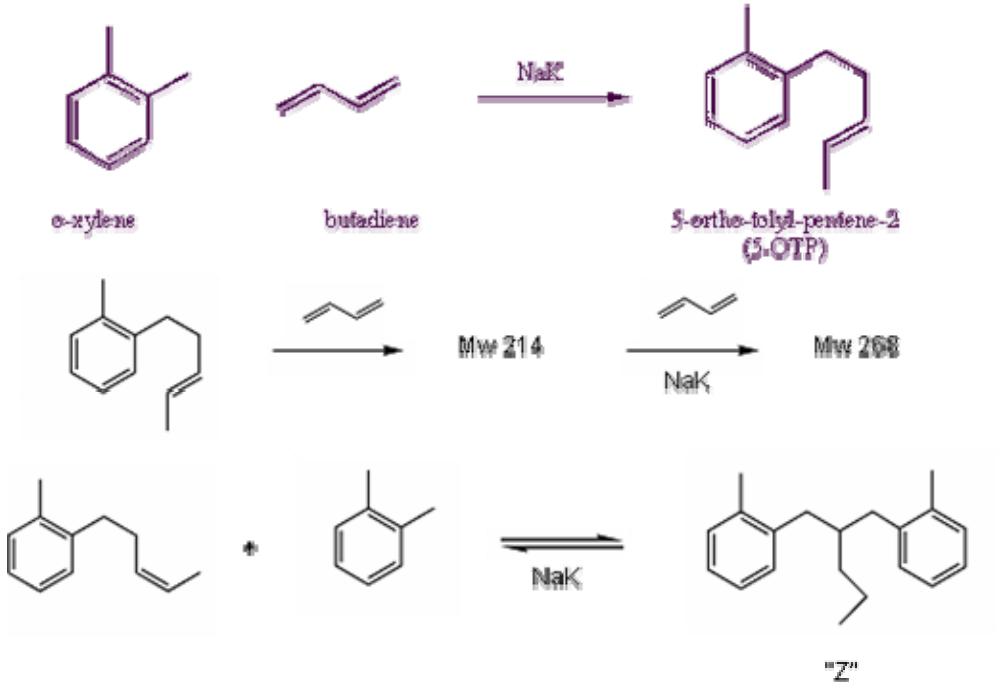

Scheme 3.2: Alkenylation of *o*-xylene with butadiene to give 5-ortho-tolyl-pent-2-ene and heavy byproducts.

3.2.3 Semi—batch alkenylation over supported catalysts

During the alkenylation of *o*-xylene with 1,3-butadiene over thermally decomposed alkali—metal azide impregnated zeolites, the reaction solution was nearly black. Quenching of the reaction with methanol resulted in a very small amount of bubbling for (8)CsN_3/CsX. Subsequent addition of water led to the formation of a white frothy layer above the water layer. These observations indicate that some amount of zero valent metal was present in the reaction solution of thermally decomposed (8)CsN_3/CsX. Despite these indications of a metallic center in the reactive solution, successful alkenylation was observed only twice and over samples of (4)NaN_3/NaX from the same synthesis batch. Conversion of *o*-xylene in these two cases was less than one percent instead of 4% as has been previously reported.[13] However, a light red solution was observed during the reaction, indicative of leaching of the active site to form an organo—alkali species in solution[13,37] and consistent with the observations of Doskocil.[13] Selectivity to 5-OTP after 8 hours was 100%. After 28 hours, conversion did not increase, but selectivity to 5-OTP decreased to 92%, indicating that the reaction had stalled.

Attempts at reproducing catalytic activity were unsuccessful, even for catalysts synthesized identically to the active (4)NaN_3/NaX. Multiple variations of the synthesis procedure, outlined in Figure 3.2, did not yield an active catalyst. The incorporation of more strongly basic alkali—metals such as potassium and cesium did not yield an active catalyst. Variations in azide loading from 2 to 8 azides/supercage, activation temperature (380 to 550^{o}C), activation time (5 to 10 hours), and reflux time (30 minutes to 2 hours) prior to reaction did not produce an active catalyst. Martens and co-workers have shown

that rapid heating (25 K/min) results in inactive ionic clusters as opposed to catalytically active metallic clusters which are formed during the slow (1 K/min) thermal decomposition of alkali—metal azides in zeolite X.[14] Ramp rates faster than 1 K/min were therefore not investigated in the pursuit of an active catalytic material. As expected, less basic zeolite supported alkali—metal oxides derived from alkali acetate impregnation of zeolite X were also unable to catalyze the alkenylation of *o*-xylene with 1,3-butadiene.

3.2.4 Gas—phase alkenylation

To eliminate leaching of the active site into the reaction mixture and to reduce diffusional limitations on reactivity, gas—phase alkenylation was attempted. Blank runs over the catalyst packing material at reactive conditions showed no conversion of *o*-xylene. Similarly, zeolite supported alkali—metal oxides were not able to catalyze the reaction. Alkali azide impregnated carbon molecular sieves also failed to catalyze alkenylation. Zeolite supported thermally decomposed alkali—metal azides were also unable to catalyze the reaction. Variations of synthesis procedure and reaction conditions as described for semi—batch alkenylation also failed to produce an active catalyst. Variations in space velocity during activation, space velocity during reaction, and the *o*-xylene to butadiene ratio during reaction did not yield an active material.

3.2.5 Gas—phase ethylation of o-xylene and toluene

The gas phase ethylation of *o*-xylene and toluene requires a less basic catalyst than the alkenylation of *o*-xylene with 1,3-butadiene[38] and has been demonstrated using metallic sodium.[37] Mono-, di-, tri-, and tetra-ethylated products are expected from this reaction (Scheme 3.3). Blank runs over the catalyst packing material under reactive conditions showed no conversion of *o*-xylene. Only the material (4)NaN_3/NaX, which was active for semi—batch alkenylation of *o*-xylene, was active for the gas phase ethylation of *o*-xylene as shown in Table 3.4. An initial conversion of 2.5% *o*-xylene was observed at early times, but quickly decreased to less than 1%. Concomitantly, ethylation to bi- and tri-ethylated products was quickly eliminated. When the initial flow of *o*-xylene was doubled during the first ten minutes of reaction, products were observed by GC more quickly. Initial conversion was increased to 4.6%, but quickly decreased to less than 1%. The selectivity to mono-ethylated product increased to 100% as conversion decreased. When removed from the reactor, the catalyst was tan in color and showed evidence of C-H bending vibrations in its FTIR spectrum(1437 and 1394 cm^{-1}) which were not present prior to reaction. Similar to the results obtained for the semi—batch alkenylation of *o*-xylene, variations in the synthesis, thermal decomposition parameters, and reaction parameters did not lead to reactivity over any other material. As expected, occluded alkali—metal oxides were not able to catalyze ethylation. Alkali azide impregnated carbon molecular sieves were not active for ethylation.

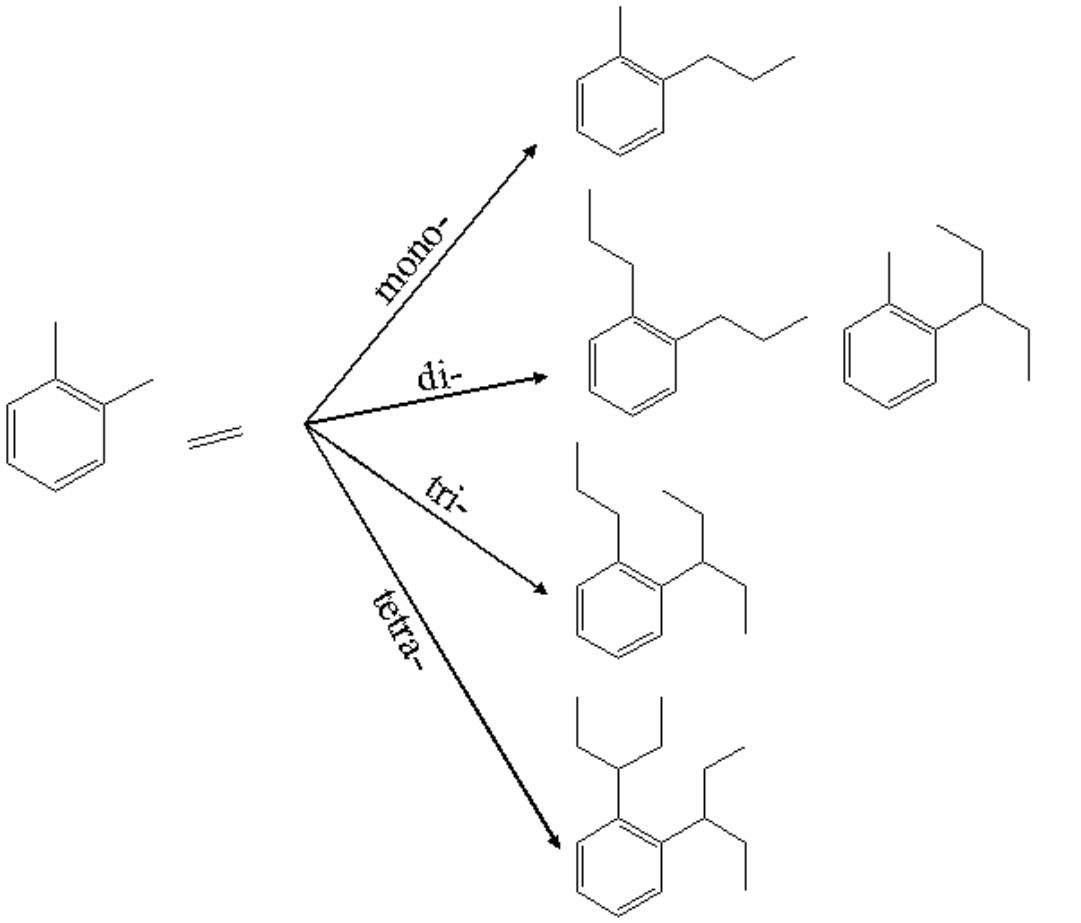

Scheme 3.2: Ethylation of *o*-xylene with butadiene to give mono-, di-, tri-, and tetra-ethylated products.

Time on stream (h)	Conv. (%)	Selectivity (%)		
		mono	bi	tri
1.5	2.5	45	25	30
1.8	1.4	68	-	32
2.3	0.7	100	-	-
2.8	0.7	100	-	-
3.2	0.5	100	-	-
0.3	4.6	84	15	1
0.8	1.7	84	16	-
1.3	1	91	9	-
1.8	0.5	100	-	-
2.2	0.4	100	-	-

Table 3.4: Results of gas phase ethylation over (4)NaN_3/NaX for two separate experiments using the same catalyst. The second data set was obtained by increasing the flow of *o*-xylene during start up.

3.2.6 Gas—phase isomerization of 1-butene

Double bond migration in butenes by metallic sodium was first observed by Pines.[39] This reaction does not require a strong basic site and can be catalyzed by zeolites exchanged with excess alkali cations,[4,38,40] alkali oxides supported in zeolites,[4,5] and by occluded alkali—metal clusters within zeolite pores.[5,14] The isomerization of 1-butene results in both *cis*- and *trans*-2-butene. The preferential formation of *cis*-2-butene is indicative of base catalyzed double bond shift as opposed to the acid catalyzed double bond shift. Results of 1-butene isomerization over alkali oxides occluded in zeolite X are shown in Table 3.5. As expected, cesium exchanged zeolite X did not show any activity towards 1-butene isomerization.[5] All other alkali oxide containing materials investigated show a

strong preference for the formation of *cis*-2-butene (cis/trans ratio > 10), indicating that the double bond shift occurs over a basic site in these materials. The material (0.4)CsO_x/CsX was the most active towards 1-butene isomerization, converting 72% of 1-butene to *cis*-2-butene with 92% selectivity after one hour on stream. The materials KO_x/KX and KO_x/NaX were decreasingly active, though more selective to *cis*-2-butene at 1 hour of reaction time. All catalysts were quickly deactivated with time.

Catalyst	Conv. (%, 1 h)	Sel Cis (%, 1 h)	Cis/Trans (1 h / max)
CsX	0	-	- / -
(0.4N)KO_x/NaX	0.22	100	infinite / infinite
(1.5N)KO_x/KX	18	100	infinite / infinite
(0.4N)CsO_x/CsX	72	93	13.1 / infinite

Table 3.5: Results of 1-butene isomerization over alkali oxide impregnated zeolite X.

The alkali azide impregnated materials showed no activity towards the double bond shift of 1-butene. Variations in synthesis procedure, thermal activation time and temperature, and reactive flows did not result in activity for the azide containing materials.

3.2.7 Summary of reactivity studies

The combined reactivity results for the isomerization of 1-butene, ethylation of *o*-xylene and toluene, and the alkenylation of 1,3-butadiene show that the alkali—metal azide impregnated zeolite does not reliably produce an active basic material. Furthermore, the inability of the materials to catalyze the weakly basic isomerization of 1-butene indicates

that the active site in the materials is either inaccessible or incompletely formed during thermal activation.

3.3 References

(1) Tsapatsis, M.; Lovallo, M.; Davis, M. E. *Microporous Materials* 1996, *5*, 381-388.

(2) Tsapatsis, M.; Okubo, T.; Lovallo, M.; Davis, M. E. MRS Symposium, 1995; p 371.

(3) Tsapatsis, M.; Lovallo, M.; Okubo, T.; Davis, M. E.; Sadakata, M. *Chemistry of Materials* 1995, *7*, 1734-1741.

(4) Kim, J. C.; Li, H.; Chen, C.; Davis, M. E. *Microporous Materials* 1994, *2*, 413-423.

(5) Bordawekar, S. V.; Davis, R. J. *Journal of Catalysis* 2000, *189*, 79-90.

(6) Hathaway, P. E.; Davis, M. E. *Journal of Catalysis* 1989, *116*, 263-278.

(7) Beres, A.; Hannus, I.; Kiricsi, I. *Journal of Thermal Analysis* 1996, *46*, 1301-1311.

(8) Martens, L. R. M.; Grobert, P. J.; Jacobs, P. A. *Nature* 1985, *315*, 568-570.

(9) Hannus, I.; Nagy, J. B.; Kiricsi, I. *Hyperfine Interactions* 1996, *99*, 409-414.

(10) Hannus, I.; Beres, A.; Nagy, J. B.; Halasz, J.; Kiricsi, I. *Journal of Molecular Structure* 1997, *410-411*, 43-46.

(11) Xu, B.; Kevan, L. *Journal of Physical Chemistry* 1992, *96*, 2642-2645.

(12) Blatter, F.; Blazey, K. W.; Portis, A. M. *Physical Review B* 1991, *44*, 2800-2802.

(13) Doskocil, E. J.; Davis, R. J. *Journal of Catalysis* 1999, *188*, 353-364.

(14) Martens, L. R. M.; Grobet, P. J.; Walter, J. M.; Vermeiren, W. J. M.; Jacobs, P. A. *Studies in Surface Science and Catalysis* 1986, *28*, 935-941.

(15) Amorureux, J.-P.; Fernandex, C.; Steuernagel, S. J. *Journal of magnetic resonance, Series A* 1996, *123*, 116-118.

(16) Brock, M.; Edwards, C.; Forster, H.; Schroder, M., 1994; p 1515-1522.

(17) Hannus, I.; Tasi, G.; Kiricsi, I.; Nagy, J. B.; Forster, H.; Fejes, P. *Thermochimica Acta* 1995, *249*, 285-294.

(18) Martens, L. R. M.; Vermeiren, W. J. M.; Grobet, P. J.; Jacobs, P. A. Studies in Surface Science and Catalysis, Louvaeuve, 1987; p 531-541.

(19) Hannus, I.; Kiricsi, I.; Varga, K.; Fejes, P. *Reaction Kinetics and Catalysis Letters* 1979, *12*, 309-314.

(20) Kiricsi, I.; Hannus, I.; Kiss, A.; Fejes, P. *Zeolites* 1982, *2*, 247-251.

(21) Olson, D. H. *Zeolites* 1995, *15*, 439-443.

(22) Caldarelli, S.; Buchholz, A.; Hunger, M. *Journal of the American Chemical Society* 2001, *123*, 7118-7123.

(23) Lim, K. H.; Grey, C. P. *Journal of the American Chemical Society* 2000, *122*, 9768-9780.

(24) Feuerstein, M.; Hunger, M.; Engelhardt, G. *Solid State Nuclear Magnetic Resonance* 1996, *7*, 95-103.

(25) Hunger, M.; Schenk, U.; Buchholz, A. *Journal of Physical Chemistry B* 2000, *104*, 12230-12236.

(26) Anderson, P. A.; Edwards, P. P. *Journal of the American Chemical Society* 1992, *114*, 10608-10618.

(27) Grey, C. P.; Poshni, F. I.; Gualtieri, A. F.; Norby, P.; Hanson, J. C.; Corbin, D. R. *Journal of the American Chemical Society* 1997, *119*, 1981-1989.

(28) Norby, P.; Poshni, F. I.; Gualtieri, A. F.; Hanson, J. C.; Grey, C. P. *Journal of Physical Chemistry B* 1998, *102*, 839-856.

(29) Xu, B.; Kevan, L. *Journal of the Chemical Society, Faraday Transactions* 1991, *87*, 2843-2847.

(30) Nakayama, H.; Klug, D. D.; Ratcliffe, C. I.; Ripmeester, J. A. *Journal of the American Chemical Society* 1994, *116*, 9777-9778.

(31) Harrison, M. R.; Edwards, P. P.; Klinowski, J.; Thomas, J. M. *Journal of Solid State Catalysis* 1984, *54*, 330-341.

(32) Rachdi, F.; Menorval, L. C. d. 13th International Zeolite Conference, Montpellier, France, 2001.

(33) Anderson, P. A. *Molecular Sieves* 2002, *3*, 307-338.

(34) Grobet, P. J.; Gorp, G. v.; Martens, L. R. M.; Jacobs, P. A. XXIII Congress Ampere on Magnetic Resonance, Rome, Italy, 1986; p 356-357.

(35) Rimai, L.; Bloembergen, N. *Journal of Physics and Chemistry of Solids* 1960, *13*, 257-270.

(36) Lillwitz, L. D. *Applied Catalysis A* 2001, *221*, 337-358.

(37) Pines, H.; Vesely, J. A.; Ipatieff, V. N. *Journal of the American Chemical Society* 1954, *77*, 554-559.

(38) Martens, L. R.; Vermeiren, W. J.; Huybrechts, D. R.; Grobet, P. J.; Jacobs, P. A. Proceedings, 9th International Congress on Catalysis, Calgary, 1988; p 420-428.

(39) Pines, H.; Vesely, J. A.; Ipatieff, V. N. *Journal of the American Chemical Society* 1955, *77*, 347-348.

(40) Tsuji, H.; Yagi, F.; Hattori, H. *Chemistry Letters* 1991, 1881-1884.